ACS APPLIED MATERIALS & INTERFACES

Research Article

www.acsami.org

Improved Dielectric Properties and Energy Storage Density of Poly(vinylidene fluoride-*co*-hexafluoropropylene) Nanocomposite with Hydantoin Epoxy Resin Coated $BaTiO_3$

Hang Luo, Dou Zhang,* Chao Jiang, Xi Yuan, Chao Chen,* and Kechao Zhou

State Key Laboratory of Powder Metallurgy, Central South University, Changsha, Hunan 410083, China

Supporting Information

ABSTRACT: Energy storage materials are urgently demanded in modern electric power supply and renewable energy systems. The introduction of inorganic fillers to polymer matrix represents a promising avenue for the development of high energy density storage materials, which combines the high dielectric constant of inorganic fillers with supernal dielectric strength of polymer matrix. However, agglomeration and phase separation of inorganic fillers in the polymer matrix remain the key barriers to promoting the practical applications of the composites for energy storage. Here, we developed a low-cost and environmentally friendly route to modifying $BaTiO_3$ (BT) nanoparticles by a kind of water-soluble hydantoin epoxy resin. The modified BT nanoparticles exhibited homogeneous dispersion in the ferroelectric polymer poly(vinylidene fluoride-*co*-hexafluoropropylene) (P(VDF-HFP)) matrix and strong interfacial adhesion with the polymer matrix. The dielectric constants of the nanocomposites increased significantly with the increase of the coated BT loading, while the dielectric loss of the nanocomposites was still as low as that of the pure P(VDF-HFP). The energy storage density of the nanocomposites was largely enhanced with the coated BT loading at the same electric field. The nanocomposite with 20 vol % BT exhibited an estimated maximum energy density of 8.13 J cm^{-3}, which was much higher than that of pure P(VDF-HFP) and other dielectric polymers. The findings of this research could provide a feasible approach to produce high energy density materials for practical application in energy storage.

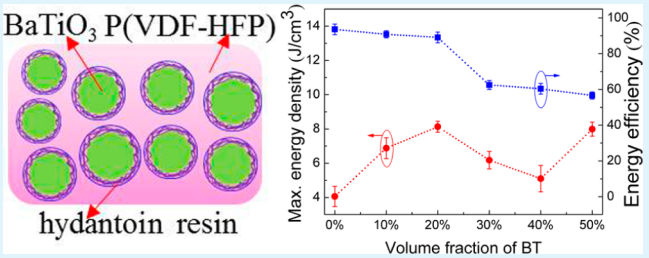

KEYWORDS: *energy storage, nanocomposites, $BaTiO_3$, hydantoin epoxy resins, ferroelectric polymers*

1. INTRODUCTION

As fossil energy is producing unavoidable pollution and facing exhaustion in the near future at the current consumption rate, renewable energy and high energy density storage technology have attracted ever-increasing attention and developed rapidly in recent years.[1,2] To meet the demands of large-scale practical applications, there has been an ever-increasing and urgent need to satisfy the low cost and environmental benignity in the processing.[1−4] 0−3 type inorganic-polymer composites (zero-dimensional fillers in a three-dimensionally connected polymer matrix) are considered to be one of the most promising high energy density materials. Because they simultaneously hold high dielectric strength and excellent processability owing to their polymeric nature, which overcome the limitations associated with the conventional inorganic dielectric materials.[5−8] The applications of dielectric materials in advanced electronic devices and electric power systems such as embedded capacitors, multilayer capacitors, and gate insulators in organic field-effect transistors are usually required to afford high energy density and low electric loss.[9−15] However, the homogeneous dispersion of nanoparticles in polymers and the strong interfacial adhesion between nanoparticles with polymer matrix are of great challenges because of the high surface energy of the inorganic nanoparticles.[16,17] Moreover, a high volume fraction of nanoparticles is usually required to obtain a high dielectric constant, which brings tougher problems on uniform dispersion. The agglomeration of inorganic nanoparticles and phase separation between fillers and matrix lead to cracks and void defects in the composites, resulting in reduced dielectric strength and energy density.[18]

Efforts on mitigating the problems of the inorganic-polymer composites in a controllable way were made extensively, focusing mostly on chemical modification methods, for example: (i) surface modication by some specific molecules such as silanes,[19] phosphonic acid,[10] and ethylene diamine[20]; (ii) encapsulation by smaller metal oxide[21]; and (iii) in situ polymerization on the surfaces of the nanoparticles.[18,22−26] Silane coupling agent was often used to modify nanoparticles to improve the dispersion of the fillers in polymer matrix. However, the unabsorbed residual species would lead to high leakage current and dielectric loss.[19] Core−shell structured nanoparticles synthesized via layer-by-layer coating with metal

Received: January 20, 2015
Accepted: March 30, 2015
Published: March 30, 2015

DOI: 10.1021/acsami.5b00555
ACS Appl. Mater. Interfaces 2015, 7, 8061−8069

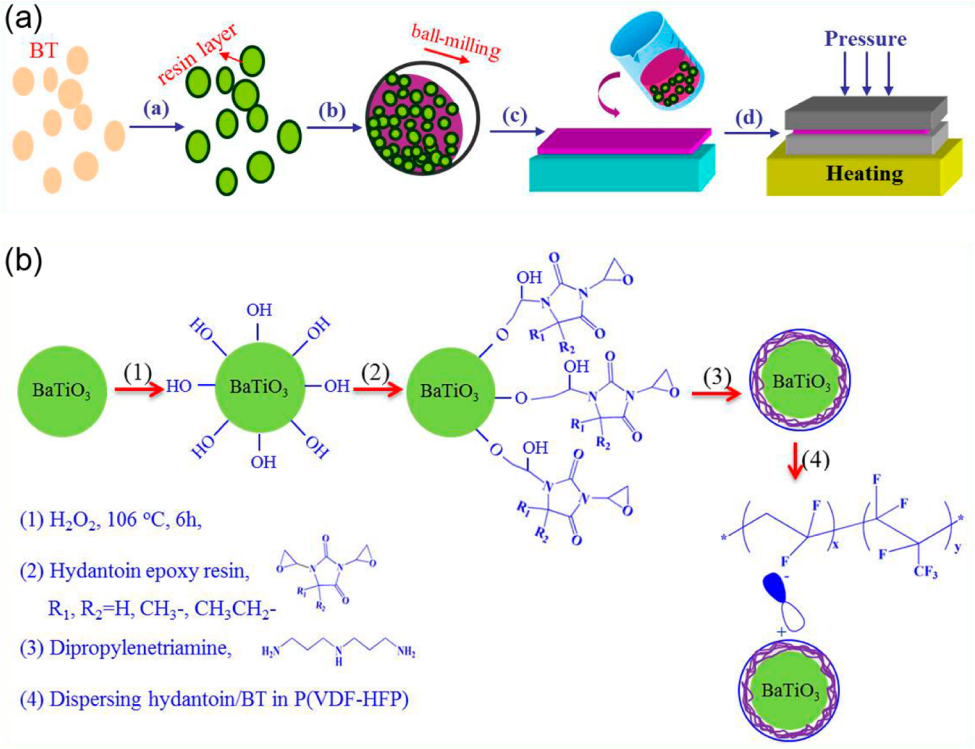

Figure 1. Schematic illustration of preparation procedures for (a) hydantoin/BT−P(VDF-HFP) nanocomposites and (b) hydantoin/BT nanoparticles.

oxide avoided introducing deleterious agents in the composites. But the preparation process of the core−shell structure was complicated and the energy storage density needed further improvement.[21] Recently, surface functionalization of the inorganic particles through grafting of specific organic molecules by in situ atom-transfer radical polymerization (ATRP) was considered to be an effective way to improve dispersion of the fillers and decrease the probability of voids or other defects at the interface between the fillers and polymer matrix.[27] As a result, fillers with the controllable core−shell structures and the composites with regulated dielectric constant and superior low dielectric loss was obtained.[24,27,28] Although the ATRP is fit for the synthesis of polymers with well-defined compositions, architectures, and functionalities,[29] the synthesis condition is difficult to realize and unsuitable for large-scale practical application.[30,31] Most of the above-mentioned techniques for modifying the inorganic particles are complicated and cannot avoid the organic solvent, which is generally expensive and energy-intensive and exerts serious concerns on human health and the environment.[32] Therefore, there is an urgent requirement to search for an economically viable and environmentally beneficial way for preparing high energy density nanocomposites.

Epoxy resins have been widely applied in the field of electronic packaging and electrical insulation because of their simplicity and high insulative properties and are lightweight.[33] Hydantoin epoxy resin is a kind of water-soluble industrial raw material with low cost and nontoxicity, which enable the process of the modified BT nanoparticles to be solvent-free.[34,35] In this paper, we reported a novel approach to prepare high energy density nanocomposites. BT nanoparticles were initially modified by hydantoin epoxy resins and introduced into ferroelectric polymer poly(vinylidene fluoride-*co*-hexafluoropropylene) (P(VDF-HFP)). Ferroelectric $BaTiO_3$ (BT) ceramics were selected as the fillers owing to the high dielectric constant and relatively low dielectric loss.[36−39] P(VDF-HFP) was employed as the polymer matrix because PVDF and its copolymer possess higher dielectric constant than other polymers,[40−43] which can better capitalize upon the fillers' dielectric constant, and thus serve as an effective way to enhance the energy storage of the nanocomposites.[44] The BT nanoparticles modified by hydantoin epoxy resin dispersed homogeneously in the P(VDF-HFP) matrix and had strong interfacial adhesion with the polymer matrix. The energy density storage of the nanocomposites was increased to 1.99 J cm^{-3}, and it is 2.5 times higher than that of the pure P(VDF-HFP) matrix (0.57 J cm^{-3}) at the electric field of 160 kV mm^{-1}. The dielectric loss was less than 0.046 in the frequency range of 1−10 kHz at room temperature.

2. EXPERIMENTAL SECTION

2.1. Functionalization of the BT Nanoparticles. Twenty grams of BT nanoparticles (Aladdin, 99%) were added into a 100 mL aqueous solution of H_2O_2 (Guoyao from China, 30 wt %) in a round-bottomed flask. The mixture was sonicated for 30 min and refluxed at 106 °C for 6 h. The nanoparticles were recovered by centrifugation at 9000 rpm for 5 min. The obtained BT nanoparticles were washed with deionized water two times with centrifugation at 1000 rpm and then dried under vacuum at 80 °C for 12 h. Subsequently, 5 g of hydantoin epoxy resins (Wuxi Meihua Chemical Co., Ltd., 99%) and moderate sulfuric acid were dissolved in deionized water and mixed with 10 g of BT nanoparticles treated by H_2O_2, followed by stirring and heating for 2 h. Then 0.5 g of dipropylenetriamine (TCI, Shanghai, 99%) was added into the mixed suspension and stirred at room temperature for 20 h, and then it was stirred at 80 °C for 2 h. The functional BT nanoparticles were recovered by centrifuging at 2000 rpm for 2

DOI: 10.1021/acsami.5b00555
ACS Appl. Mater. Interfaces 2015, 7, 8061−8069

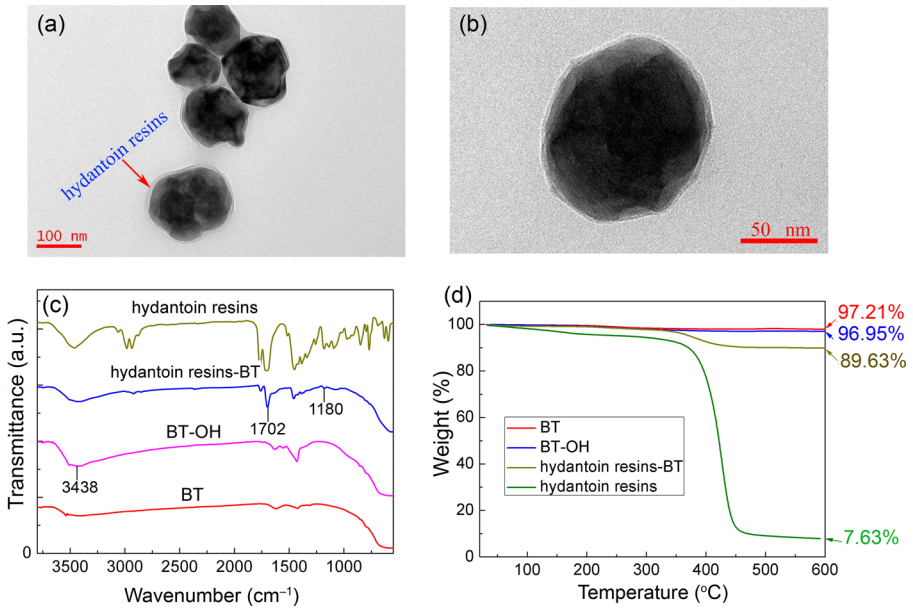

Figure 2. (a,b) TEM images of hydantoin/BT, (c) FT-IR spectra of the pure hydantoin epoxy resins, hydantoin/BT, BT−OH, and BT, and (d) TGA curves for the BT, BT−OH, hydantoin/BT, and pure hydantoin epoxy resin.

min, washed with deionized water two times, and finally dried under vacuum at 80 °C for 12 h. For comparison, the BT nanoparticles untreated by H_2O_2 reacted with hydantoin epoxy resin by a similar method.

2.2. Preparation of Nanocomposites with Hydantoin Epoxy Resin Coated BT. Hydantoin epoxy resin coated BT (hydantoin/BT) was ball-milled in *N*,*N*-dimethylformamide (DMF) (Guoyao, China) for 2 days and mixed with P(VDF-HFP) (Aldrich, pellets with less than 15% HFP) for another 5 days by ball-milling. The resultant suspension was then cast onto a clean glass and dried at 80 °C for 12 h under vacuum. The dried nanocomposite sheets were compressed into films at 200 °C under a pressure of about 15 MPa. The thickness of the final composite film was about 10−20 μm. Gold electrodes of about 40 nm in thickness were sputtered on both sides of the film using a mask with 2 mm diameter eyelets.

The fabrication process of hydantoin/BT−P(VDF-HFP) nanocomposites is shown in Figure 1a. First, the BT nanoparticles were coated by a hydantoin epoxy resin layer. Second, the functional BT nanoparticles were dispersed in the P(VDF-HFP) solution by ball-milling. Afterward, the uniform suspension was cast onto a glass plate to form the nanocomposite sheets. Finally, the nanocomposite sheets were compressed into compact films by hot-pressing. The detailed modification process of the BT nanoparticles is shown in Figure 1b. As can be seen, the BT nanoparticles were pretreated by H_2O_2 to increase the amount of hydroxyl on the surfaces of BT nanoparticles.[24,27] Subsequently, with the addition of hydantoin epoxy resins, a ring-opening reaction was carried out between the epoxide group of the resin and hydroxyl groups on the surfaces of BT−OH. The addition of the curing agent dipropylenetriamine led to the cross-linking and the solidification reactions of the hydantoin epoxy resins. Some epoxide groups of the hydantoin epoxy resin firmly combined with the hydroxyl of BT−OH and others carried out the reaction of ring-opening polyaddition with the hydrogen of amine groups. The goal productions were easily synthesized because of the high activity of epoxide group and hydrogen of amine.[41,45] Naturally, dense organic membranes were coated on the surface of BT.

2.3. Characterization. Transmission electron microscopy (TEM) images were obtained from a JEOL JEM-2100 instrument operated at an accelerating voltage at 200 kV. The samples were prepared by dropping the sample solutions onto carbon-coated copper grids and air-drying before measurement. The crystal structure of the nanocomposites was examined in θ−2θ mode by X-ray diffraction (XRD, Rigaku D-Max/2550VB$^+$) utilizing Cu Kα radiation (λ = 1.5418 Å). Fourier-transform infrared (FT-IR) spectroscopy was performed with a Nicolet 6700 instrument over the range of 4000−450 cm^{-1} to determine the functionalization of the samples. Thermogravimetric analysis (TGA, NETZSCH STA 449) was conducted at a heating rate of 10 °C min^{-1} in a nitrogen flow (20 mL min^{-1}). The morphology of the composites was performed by scanning electron microscopy (SEM, JSM-6390). Frequency-dependent dielectric constant and dielectric loss were measured using an Agilent 4294A LCR meter with a frequency range from 1 kHz to 10 MHz. Electric displacement−electric field loops and leakage current were measured by a Precision Premier II ferroelectric polarization tester (Radiant, Inc.) at room temperature and 100 Hz.

3. RESULTS AND DISCUSSION

3.1. Characterization of the Hydantoin/BT and the Nanocomposite. Figure 2a,b displays the TEM images of the BT nanoparticles coated with hydantoin epoxy resins. A resin layer can be clearly observed on the surfaces of the BT nanoparticles compared to the pure BT (see Figure S1 in the Supporting Information). The FT-IR spectra of pure hydantoin epoxy resins, hydantoin/BT, BT−OH, and BT are shown in Figure 2c. Since BT nanoparticles lack reactive functional groups on their surface, e.g., −OH, it is difficult to form chemical bonds with modification agents.[24] For comparison, the results of FT-IR and TGA of the BT nanoparticles unmodified by H_2O_2 reacted with hydantoin epoxy resins are shown in Figure S2 (Supporting Information). As can be seen,

DOI: 10.1021/acsami.5b00555
ACS Appl. Mater. Interfaces 2015, 7, 8061−8069

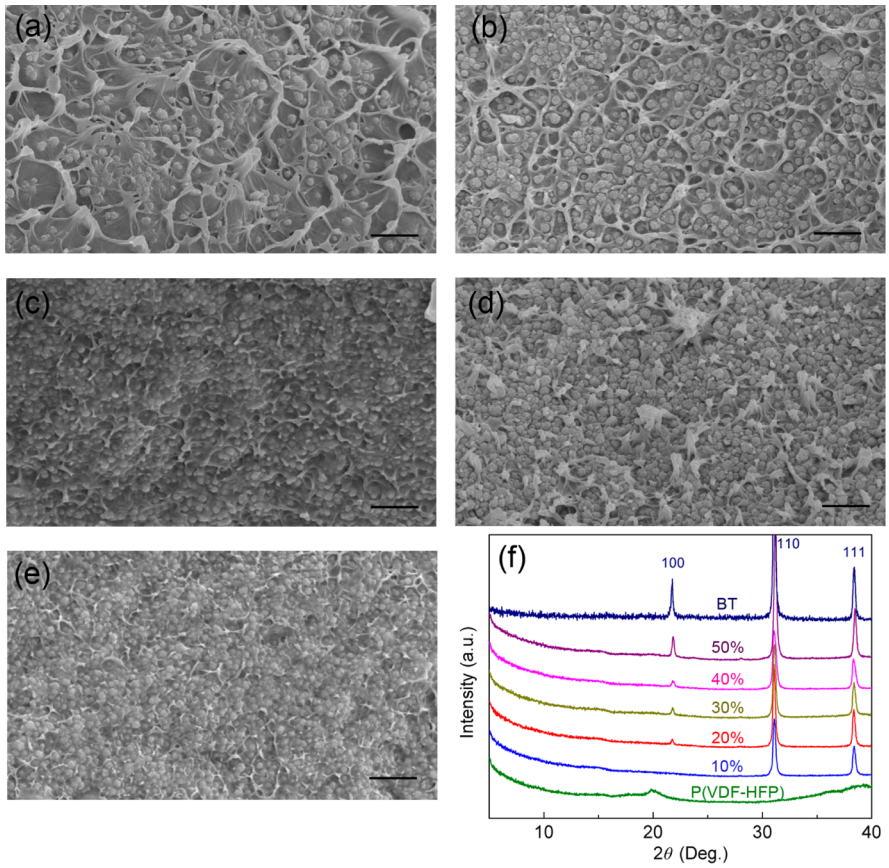

Figure 3. SEM images of the cross sections of hydantoin/BT−P(VDF-HFP) nanocomposite films with different nanoparticle volume fractions. Scale bars are 1 μm. (f) XRD patterns of BT nanoparticles, pure P(VDF-HFP), and hydantoin/BT−P(VDF-HFP) nanocomposites with different volume fractions of BT.

there is no characteristic peak in the cures of FT-IR of the sample and the weight loss of the sample is nearly equal to the pure BT. Thus, it is necessary to modify the BT nanoparticles by H_2O_2. After treatment by H_2O_2, an obvious broad absorption band at about 3438 cm^{-1} appeared in the spectra, which came from the contribution of −OH in BT−OH. Both hydantoin epoxy resins and hydantoin/BT showed a similar absorption peak at about 1702 cm^{-1}, which is due to C═O stretching vibrations. However, no peak appeared in the curve of BT at 1702 cm^{-1}. The absorption bands at 1180 cm^{-1} originate from the O−C stretching vibrations, which suggest that the tight chemical bond was formed between the epoxide group of hydantoin epoxy resins and −OH of BT−OH. These results indicated that the hydantoin epoxy resin was successfully coated to the surface of BT nanoparticles. Figure 2d shows the TGA curves of BT, BT−OH, hydantoin/BT, and pure hydantoin epoxy resins. The weight loss below 100 °C was attributed to the deintercalation of water. The dramatic weight loss from 350 to 450 °C resulted from the thermal decomposition of organic resin.[27] The weight residues of hydantoin/BT were attributed to BT because the weight loss of pure hydantoin epoxy resins was almost 92.4%; thus, the weight loss of hydantoin/BT nearly equaled the amount of resin coated on the surface of BT.

Figure 3a−e shows the SEM images of the cross sections of the hydantoin/BT−P(VDF-HFP) nanocomposite films with different BT contents. The SEM images of the surface morphology of the nanocomposites are shown in Figure S3 in the Supporting Information). As can be seen in Figure 3a, a small quantity of BT nanoparticles were embedded in the polymer matrix with no obvious agglomeration and defects when the BT content was 10 vol %. There were more and more BT nanoparticles in the composites and the distances between nanoparticles became much closer with the increase of BT content, especially for the samples with 50 vol % BT nanoparticles. Because of the presence of a strong electron-withdrawing functional group (−C−F) of P(VDF-HFP), hydantoin/BT bonds tightly with the polymer host.[46] Thus, the BT nanoparticles maintained a homogeneous dispersion in the composites and neglected evidence of defects was observed between both particle−particle and particle−matrix, indicating strong interfacial bonding and excellent compatibility between nanoparticles and the P(VDF-HFP) matrix. The results can be further proved by the high-magnification SEM images of the nanocomposites (Figure S4 in the Supporting Information). Uniform dispersion of the BT nanoparticles in P(VDF-HFP) matrix ensures high energy density as well as reproducibility of the nanocomposites. Figure 3f shows the XRD patterns of BT nanoparticles, pure P(VDF-HFP), and hydantoin/BT−P(VDF-HFP) nanocomposites with different amounts of BT content. It can be seen that the XRD pattern of the pure P(VDF-HFP) exhibited an intense scattering background and a wide hump at about 20°, which was a typical feature of amorphous structure, while the XRD pattern of BT powders displayed a perovskite phase with three distinguished diffraction peaks in the detected range. Both diffraction peaks from perovskite structure and scattering hump from P(VDF-HFP) matrix can be observed in the nanocomposite films. With the increase of BT contents, the

DOI: 10.1021/acsami.5b00555
ACS Appl. Mater. Interfaces 2015, 7, 8061−8069

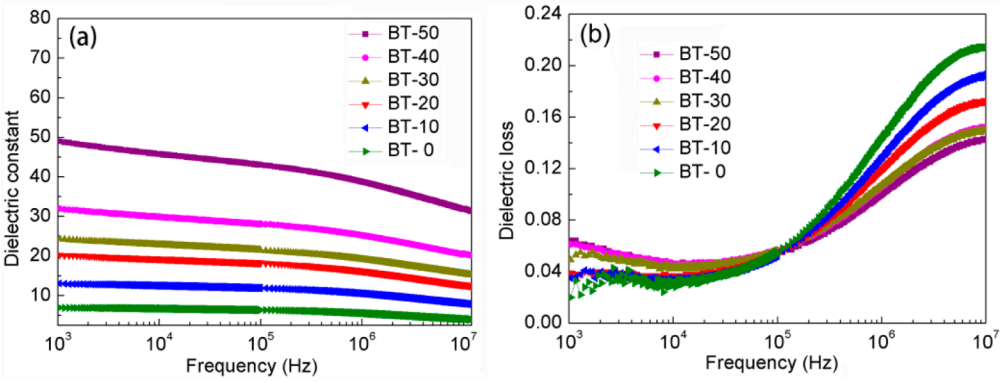

Figure 4. Frequency dependence of (a) dielectric constant and (b) dielectric loss of the hydantoin/BT−P(VDF-HFP) nanocomposites at room temperature.

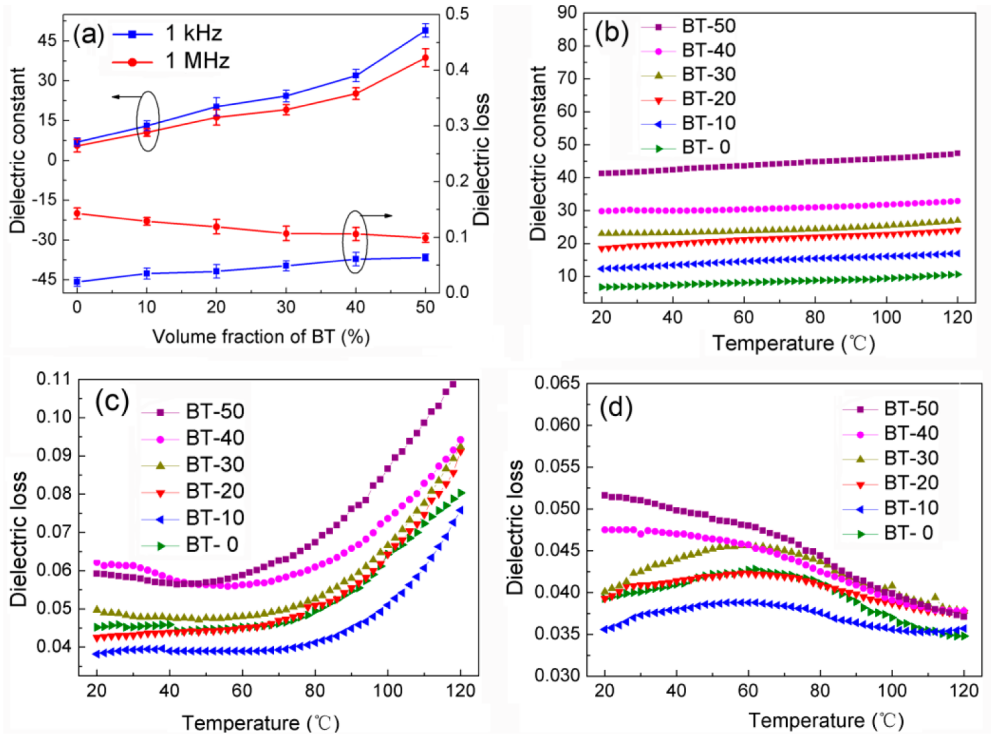

Figure 5. (a) Dielectric properties of the nanocomposites as a function of the volume fraction of BT at room temperature. Temperature dependence of (b) dielectric constant at 1 kHz and dielectric loss at (c) 1 kHz and (d) 100 kHz.

intensity of (100) and (111) diffraction peaks increased gradually while the characteristics of amorphous scattering became negligible of the nanocomposites, indicating accurate component control of the nanocomposites.[47]

3.2. Dielectric Properties of the Nanocomposites. Figure 4 shows the dielectric properties of hydantoin/BT−P(VDF-HFP) nanocomposite films as a function of frequency over the range of 1 kHz to 10 MHz. As is shown in Figure 4a, the dielectric constant of the nanocomposites decreased with the increase of the frequency. For example, the dielectric constant was 48.9 at 1 kHz of the sample with 50 vol % BT, and it was reduced to 31.9 at 10 MHz. However, the dielectric loss of the nanocomposites shows a different tendency (Figure 4b). It can be seen that the dielectric losses slightly decreased in the frequency range from 1 to 10 kHz. For instance, the dielectric loss of the nanocomposite with 50 vol % BT was 0.060 at 1 kHz and decreased slightly (0.046) at 10 kHz. The dielectric losses of all nanocomposites remained stable up in the frequency range from 10 to 100 kHz, and then an obvious increase appeared in the high-frequency range (>100 kHz), which were mainly due to the α_a relaxation of the P(VDF-HFP) matrix.[13,40,48−50] The dielectric losses of all the samples were less than 0.065 (<100 kHz), which was attributed to the factors including the insulating polymer shells on BT nanoparticles, homogeneous dispersion of BT nanoparticles in the P(VDF-HFP) matrix, and a higher fraction of isotactic structure of the P(VDF-HFP) matrix in the composites than that of pure P(VDF-HFP).[27]

The dielectric properties of the samples as a function of the volume fraction of BT at 1 kHz and 1 MHz are shown in Figure 5a. It can be seen that the dielectric constants increased sharply with the increase of the BT volume fraction at both frequencies. Specifically, the dielectric constant increased from 6.9 to 48.9 and 5.5 to 38.7 as the BT content increased from 0 to 50 vol % at 1 kHz and 1 MHz, respectively. Similar results have been reported previously.[24,36] The dielectric loss of the nano-

DOI: 10.1021/acsami.5b00555
ACS Appl. Mater. Interfaces 2015, 7, 8061−8069

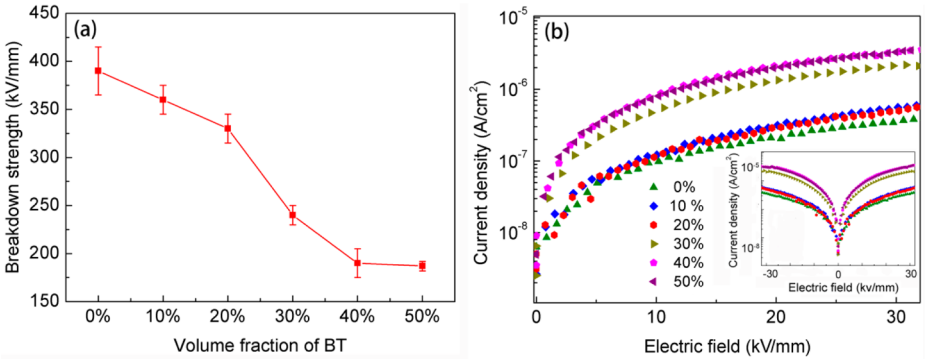

Figure 6. (a) Breakdown strength and (b) electric field dependence of current density of the hydantoin/BT−P(VDF-HFP) nanocomposites with 0−50% volume fractions of BT.

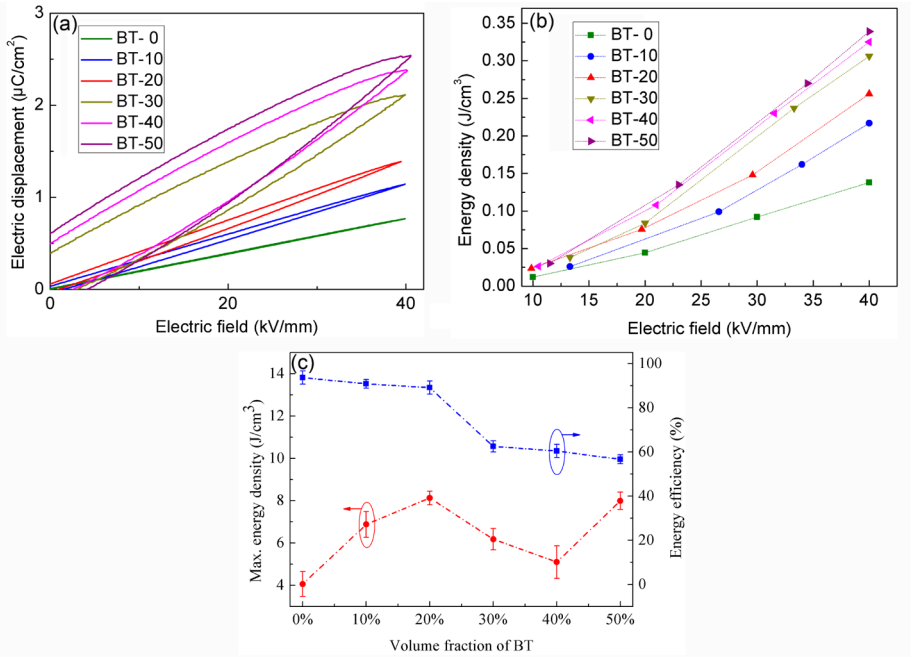

Figure 7. (a) *D*−*E* loops, (b) the dependence of energy density on the different volume fractions of hydantoin/BT in the P(VDF-HFP) matrix with varying electric field, and (c) maximum energy density and the energy efficiency as a function of the hydantoin/BT volume fraction.

composites exhibits different tendencies with the BT content at 1 kHz and 1 MHz. At the frequency of 1 kHz, the dielectric loss increased from 0.020 to 0.064 with the increase of BT loading, which was due to the increased defects in the nanocomposites.[51,52] However, the tendency of dielectric loss was reversed (from 0.140 to 0.090) at the frequency of 1 MHz because the electric conduction and dipolar polarization at high frequency would restrict the motion of the polymer chain.[16,24,40]

The temperature dependence of the dielectric constant of the samples is shown in Figure 5b. The dielectric constant increased by small amounts with the increase of the temperature. For example, the dielectric constant of the nanocomposite with 50 vol % BT was 41.3 at 20 °C, and gradually increased to 47.2 at 120 °C. This phenomenon was due to the Maxwell−Wagner−Sillars (MWS) interfacial polarization. Because BT and P(VDF-HFP) in the nanocomposite have different dielectric properties, which resulted in the interfacial polarization, the dielectric constant increased with the increase of temperature.[15] The dielectric loss as a function of volume fraction of BT over the temperature range from 20 to 120 °C at 1 kHz and 1 MHz are shown in parts (c) and (d), respectively, of Figure 5. It can be seen that the BT-10 sample has the lowest dielectric loss at the frequencies of both 1 kHz and 100 kHz. The reason is that the sample of BT-10 had a fewer molecular dipoles due to the reduction of polymer matrix compared with the pure P(VDF-HFP). Besides, the introduction of BT nanoparticles with insulating shell to the polymer matrix restricted the migration and accumulation of the space charge within the composite.[36] At 1 kHz, the dielectric loss of the nanocomposites changed slightly at temperature less than ∼60 °C, but increased when the temperature was above 60 °C. However, at 100 kHz, the change of dielectric loss scattered the nanocomposites with the increase of temperature (Figure 5d). For example, the dielectric loss of the nanocomposites with 50 vol % BT decreased monotonically while that of 20 vol % BT sample varied slightly with the temperature. At 1 kHz, the interfacial polarization originated from the different dielectric loss of the BT and polymer matrix in the nanocomposite, which would lead to an easier space charge conduction at relatively high temperature, and resulted in the increase of the dielectric loss.[15] Because of the long relaxation time, the MWS interfacial

DOI: 10.1021/acsami.5b00555
ACS Appl. Mater. Interfaces 2015, 7, 8061−8069

polarization and space charge polarization mainly work in the low-frequency range[2,19] and thus the dielectric loss varied slightly with temperature at 100 kHz.

3.3. Energy Storage Performance of the Nanocomposites. The energy density is related to not only the dielectric constant but also the breakdown strength of the nanocomposites. The results in Figure 6a show the breakdown strength with the addition of BT nanoparticles to the matrix. The breakdown strength decreased with the increase of BT loading. More specifically, the breakdown strength of pure P(VDF-HFP) was 390 kV mm^{-1}, which decreased to 187 kV mm^{-1} when the BT loading increased to 50 vol %. The phenomenon was attributed to not only the low breakdown electric field of ceramic fillers itself but also the possible percolation path through the ceramic islands in the polymer matrix.[44] The breakdown strength is strongly influenced by interface areas, agglomerations, and voids in the composites.[16,53−55] These factors result in inhomogeneous electric field breakdown strength in the polymer matrix and lead to the decrease of the effective breakdown strength of the nanocomposites.[16,56,57]

Low leakage current density is always essential for the application of dielectric materials in energy storage.[58] The characteristic of leakage current density over a wide range of electric fields is shown in Figure 6b. The leakage current density increased from 3.6×10^{-7} to 3.5×10^{-6} A cm^{-2} with the volume fraction of BT increased from 10% to 50%, while all of the prepared nanocomposites showed low leakage current density under 30 kV mm^{-1} at room temperature and the largest leakage current density was less than 3.5×10^{-6} A cm^{-2}. It is proposed that the high breakdown strength and relatively low leakage current density of the hydantoin/BT−P(VDF-HFP) nanocomposites are attributed to the uniform and high-quality nanocomposite films.[58]

Typical electric displacement−electric field (D−E) loops of the hydantoin/BT−P(VDF-HFP) nanocomposites measured at various volume fractions of BT is shown in Figure 7a. The electric displacement increased notably with the increase of the contents of BT fillers under the same electric field. The maximum electric displacement of pure P(VDF-HFP) was 0.74 μC cm^{-2}. With increasing of the BT contents, the maximum electric displacement increased monotonically and reached 2.53 μC cm^{-2} for the nanocomposite with 50 vol % BT loading. According to the formula $D = \varepsilon_0\varepsilon_r E$, where ε_0 and ε_r are permittivity of vacuum and dielectric constant of the composites, respectively, the increased electric displacement is attributed to the increase of dielectric constant of the nanocomposites.

On the basis of definition of energy storage, the energy density J ($J = \int_{D_r}^{D_{max}} E\, dD$, where D_{max} and D_r are the maximum electric displacement and remnant electric displacement, respectively) can be derived from the D−E loops.[59,60] The energy density of the samples as a function of electric field is shown in Figure 7b. As can be seen, the energy density increased with the increase of electric field. For example, the energy density of the sample with 40 vol % BT loading increased from 0.026 J cm^{-3} at the electric field of 10 kV mm^{-1} to 0.325 J cm^{-3} at 40 kV mm^{-1}. Meanwhile, the energy density increased significantly with the increase of the BT content. The energy density of the composite with 50 vol % BT was 0.348 J cm^{-3} at 40 kV mm^{-1}, which was increased by about 150% compared with the pure P(VDF-HFP) (0.138 J cm^{-3} at 40 kV mm^{-1}).

It is necessary to obtain high energy density with high efficiency for practical applications since the energy losses often lead to heating and degenerating the performance and reliability of the materials. The energy efficiency η ($\eta = J/(J + J_{loss})$, where J and J_{loss} are energy density and energy loss, respectively) of the composites, calculated from the D−E loops, are shown in Figure 7c. Although the energy efficiency decreased gradually from 93.64% to 56.64% as the BT loading increased from 0 to 50 vol %, such energy efficiencies are generally enough for practical application.[2] The estimated maximum energy density (U_{max}) of the samples can be calculated from the equation $U_{max} = 1/2\varepsilon_0\varepsilon_r E_b^2$, where E_b is the electric breakdown strength.[36,44] The calculated maximum energy density is shown in Figure 7c in which ε_r was obtained at 1 kHz and E_b was derived from Figure 6a. It was shown that the maximum energy density was 4.06 J cm^{-3} for the pure P(VDF-HFP) and increased to 8.13 J cm^{-3} for the composite with 20 vol % BT. Then the energy density showed a relative decrease when the BT content increased to 30−40 vol %, which was due to the dramatical decrease of the breakdown strength, as shown in Figure 6a. The energy density of the composite with 50 vol % BT increased to 7.99 J cm^{-3}. According to the equation aforementioned, the high energy density of the composites was attributed to the increased dielectric constant and the endurance of high electric field. The energy density of the composite with 20 vol % BT was the highest among the six samples, which was mainly attributed to the high breakdown strength of 330 kV mm^{-1} and relatively high dielectric constant. Although the breakdown strength of the composite with 50 vol % BT decreased to 187 kV mm^{-1}, the energy density still maintained 7.99 J cm^{-3}, owing to the highest dielectric constant of 48.96.

4. CONCLUSIONS

A low-cost and environmentally friendly route was introduced to prepare high energy density nanocomposites. Compared with the traditional 0−3 type inorganic−polymer composites, the hydantoin/BT−P(VDF-HFP) nanocomposites exhibited significant superiority in overcoming the challenges of inorganic particles agglomeration and phase separation in matrixes. A series of nanocomposites were prepared based on different loadings of hydantoin/BT and P(VDF-HFP). Compared to the pure P(VDF-HFP), the dielectric constants of the nanocomposites increased significantly with the introduction of hydantoin/BT to the nanocomposites. Additionally, the dielectric losses of all nanocomposites were less than 0.065 at the frequency below 100 kHz and the hydantoin/BT nanocomposites maintained a reasonable breakdown field strength of 187 kV/mm at 50 vol % of BT. The maximum energy density of the composite with 20 vol % BT was 8.13 J cm^{-3}, which was about two times of the pure P(VDF-HFP), and the energy efficiency was beyond 56.64%. It was demonstrated that modifying inorganic particles by hydantoin epoxy resins is a potential industrial route to prepare high energy density nanocomposites.

■ ASSOCIATED CONTENT

Supporting Information

TEM and high-magnification SEM images of the pure BT, FT-IR, and TGA of the hydantoin/BT treated by H_2O_2, and hydantoin/BT untreated by H_2O_2 and BT; SEM images of the

DOI: 10.1021/acsami.5b00555
ACS Appl. Mater. Interfaces 2015, 7, 8061−8069

surfaces of hydantoin/BT−P(VDF-HFP) nanocomposite; and high-magnification SEM images of the nanocomposites. This material is available free of charge via the Internet at http://pubs.acs.org.

AUTHOR INFORMATION

Corresponding Authors

*E-mail: dzhang@csu.edu.cn (D. Zhang).
*E-mail: pkhqchenchao@126.com (C. Chen).

Author Contributions

The manuscript was written through contributions of all authors. All authors have given approval to the final version of the manuscript.

Notes

The authors declare no competing financial interest.

ACKNOWLEDGMENTS

This work was financially supported by the National Natural Science Foundation of China (no. 51072235), Hunan Provincial Natural Science Foundation of China (no. 11JJ1008), Ph.D. Programs Foundation of Ministry of Education of China (no. 20110162110044), and Defense Industrial Technology Development Program (no. A1420133028).

REFERENCES

(1) Pan, H.; Hu, Y. S.; Chen, L. Room-Temperature Stationary Sodium-Ion Batteries for Large-Scale Electric Energy Storage. *Energy Environ. Sci.* **2013**, *6*, 2338−2360.

(2) Kumar, P. S.; Sundaramurthy, J.; Subramanian, S.; Babu, V. J.; Singh, G.; Allakhverdiev, S. I.; Ramakrishna, S. Hierarchical Electrospun Nanofibers for Energy Harvesting, Production and Environmental Remediation. *Energy Environ. Sci.* **2014**, *7*, 3192−3222.

(3) Sun, Y.; Wu, Q.; Shi, G. Graphene Based New Energy Materials. *Energy Environ. Sci.* **2011**, *4*, 1113−1132.

(4) Fredin, L. A.; Li, Z.; Ratner, M. A.; Lanagan, M. T.; Marks, T. J. Enhanced Energy Storage and Suppressed Dielectric Loss in Oxide Core−Shell-Polyolefin Nanocomposites by Moderating Internal Surface Area and Increasing Shell Thickness. *Adv. Mater.* **2012**, *24*, 5946−5953.

(5) Tang, H. X.; Zhou, Z.; Sodano, H. A. Relationship between $BaTiO_3$ Nanowire Aspect Ratio and the Dielectric Permittivity of Nanocomposites. *ACS Appl. Mater. Interfaces* **2014**, *6*, 5450−5455.

(6) Luo, S. B.; Yu, S. H.; Sun, R.; Wong, C. P. Nano Ag-Deposited $BaTiO_3$ Hybrid Particles as Fillers for Polymeric Dielectric Composites: Toward High Dielectric Constant and Suppressed Loss. *ACS Appl. Mater. Interfaces* **2014**, *6*, 176−182.

(7) Yu, K.; Niu, Y.; Bai, Y.; Zhou, Y.; Wang, H. Poly(vinylidene fluoride) polymer based nanocomposites with significantly reduced energy loss by filling with core-shell structured $BaTiO_3/SiO_2$ nanoparticles. *Appl. Phys. Lett.* **2013**, *102*, 102903.

(8) Xie, L. Y.; Huang, X. Y.; Huang, Y. H.; Yang, K.; Jiang, P. K. Core−shell Structured Hyperbranched Aromatic Polyamide/$BaTiO_3$ Hybrid Filler for Poly(vinylidene fluoride-trifluoroethylene-chlorofluoroethylene) Nanocomposites with the Dielectric Constant Comparable to That of Percolative Composites. *ACS Appl. Mater. Interfaces* **2013**, *5*, 1747−1756.

(9) Tang, H. X.; Lin, Y. R.; Sodano, H. A. Synthesis of High Aspect Ratio $BaTiO_3$ Nanowires for High Energy Density Nanocomposite Capacitors. *Adv. Energy Mater.* **2013**, *3*, 451−456.

(10) Kim, P.; Doss, N. M.; Tillotson, J. P.; Hotchkiss, P. J.; Pan, M. J.; Marder, S. R.; Li, J. Y.; Calame, J. P.; Perry, J. W. High Energy Density Nanocomposites Based on Surface-Modified $BaTiO_3$ and a Ferroelectric Polymer. *ACS Nano* **2009**, *3*, 2581−2592.

(11) Zhang, X.; Chen, W. W.; Wang, J. J.; Shen, Y.; Gu, L.; Y. Lin, H.; Nan, C. W. Hierarchical Interfaces Induce High Dielectric Permittivity in Nanocomposites Containing TiO_2@ $BaTiO_3$ Nanofibers. *Nanoscale* **2014**, *6*, 6701−6709.

(12) Wang, D. R.; Bao, Y. R.; Zha, J. W.; Zhao, J.; Dang, Z. M.; Hu, G. H. Improved Dielectric Properties of Nanocomposites Based on Poly(vinylidene fluoride) and Poly(vinyl alcohol)-Functionalized Graphene. *ACS Appl. Mater. Interfaces* **2012**, *4*, 6273−6279.

(13) Liu, S. H.; Xue, S. X.; Zhang, W. Q.; Zhai, J. W.; Chen, G. H. Significantly Enhanced Dielectric Property in PVDF Nanocomposites Flexible Films Through a Small Loading of Surface-Hydroxylated $Ba_{0.6}S_{0.4}TiO_3$ Nanotubes. *J. Mater. Chem. A* **2014**, *2*, 18040−18046.

(14) Xie, L. Y.; Huang, X.; Huang, Y. H.; Yang, K.; Jiang, P. K. Core @ Double-Shell Structured $BaTiO_3$−Polymer Nanocomposites with High Dielectric Constant and Low Dielectric Loss for Energy Storage Application. *J. Phys. Chem. C* **2013**, *117*, 22525−22537.

(15) Benhadjala, W.; Bord-Majek, I.; Béchou, L.; Suhir, E.; Buet, M.; Rougé, F.; Gaud, V.; Plano, B.; Ousten, Y. Improved performances of polymer-based dielectric by using inorganic/organic core−shell nanoparticles. *Appl. Phys. Lett.* **2012**, *101*, 142901.

(16) Yu, K.; Niu, Y. J.; Zhou, Y. C.; Bai, Y. Y.; Wang, H. Nanocomposites of Surface-Modified $BaTiO_3$ Nanoparticles Filled Ferroelectric Polymer with Enhanced Energy Density. *J. Am. Ceram. Soc.* **2013**, *96*, 2519−2524.

(17) Schroeder, R.; Majewski, L. A.; Grell, M. High-Performance Organic Transistors Using Solution-Processed Nanoparticle-Filled High-k Polymer Gate Insulators. *Adv. Mater.* **2005**, *17*, 1535−1539.

(18) Jung, H. M.; Kang, J. H.; Yang, S. Y.; Won, J. C.; Kim, Y. S. Barium Titanate Nanoparticles with Diblock Copolymer Shielding Layers for High-Energy Density Nanocomposites. *Chem. Mater.* **2009**, *22*, 450−456.

(19) Dang, Z. M.; Wang, H. Y.; Xu, H. P. Influence of Silane Coupling Agent on Morphology and Dielectric Property in $BaTiO_3$/Polyvinylidene Fluoride Composites. *Appl. Phys. Lett.* **2006**, *89*, 112902.

(20) Li, J.; Claude, J.; Franco, L. N.; Seok, S.; Wang, Q. Electrical Energy Storage in Ferroelectric Polymer Nanocomposites Containing Surface-Functionalized $BaTiO_3$ Nanoparticles. *Chem. Mater.* **2008**, *20*, 6304−6306.

(21) Li, Z.; Fredin, L. A.; Tewari, P.; DiBenedetto, S. A.; Lanagan, M. T.; Ratner, M. A.; Marks, T. J. In Situ Catalytic Encapsulation of Core−Shell Nanoparticles Having Variable Shell Thickness: Dielectric and Energy Storage Properties of High-Permittivity Metal Oxide Nanocomposites. *Chem. Mater.* **2010**, *22*, 5154−5164.

(22) Yang, K.; Huang, X. Y.; Zhu, M.; Xie, L. Y.; Tanaka, T.; Jiang, P. K. Combining RAFT Polymerization and Thiol−Ene Click Reaction for Core−Shell Structured Polymer@$BaTiO_3$ Nanodielectrics with High Dielectric Constant, Low Dielectric Loss, and High Energy Storage Capability. *ACS Appl. Mater. Interfaces* **2014**, *6*, 1812−1822.

(23) Guo, N.; DiBenedetto, S. A.; Kwon, D. K.; Wang, L.; Russell, M.; Lanagan, M.; Facchetti, A.; Marks, T. Supported Metallocene Catalysis for In Situ Synthesis of High Energy Density Metal Oxide Nanocomposites. *J. Am. Chem. Soc.* **2007**, *129*, 766−767.

(24) Xie, L. Y.; Huang, X. Y.; Yang, K.; Li, S.; Jiang, P. K. "Grafting to" Route to PVDF-HFP-GMA/$BaTiO_3$ Nanocomposites with High Dielectric Constant and High Thermal Conductivity for Energy Storage and Thermal Management Applications. *J. Mater. Chem. A* **2014**, *2*, 5244−5251.

(25) Huang, X. Y.; Iizuka, T.; Jiang, P. K.; Ohki, Y.; Tanaka, T. Role of Interface on the Thermal Conductivity of Highly Filled Dielectric Epoxy/AlN Composites. *J. Phys. Chem. C* **2012**, *116*, 13629−13639.

(26) Yang, K.; Huang, X. Y.; Xie, L. Y.; Wu, C.; Jiang, P. K.; Tanaka, T. Core−Shell Structured Polystyrene/$BaTiO_3$ Hybrid Nanodielectrics Prepared by In Situ RAFT Polymerization: A Route to High Dielectric Constant and Low Loss Materials with Weak Frequency Dependence. *Macromol. Rapid Commun.* **2012**, *33*, 1921−1926.

(27) Xie, L. Y.; Huang, X. Y.; Wu, C.; Jiang, P. K. Core-shell Structured Poly(methyl methacrylate)/$BaTiO_3$ Nanocomposites Prepared by *in-situ* Atom Transfer Radical Polymerization: a Route to

DOI: 10.1021/acsami.5b00555
ACS Appl. Mater. Interfaces 2015, 7, 8061−8069

High Dielectric Constant Materials with the Inherent Low loss of the Base Polymer. *J. Mater. Chem.* **2011**, *21*, 5897−5906.
(28) Yang, K.; Huang, X. Y.; Fang, L.; He, J.; Jiang, P. K. Fluoro-Polymer Functionalized Graphene for Flexible Ferroelectric Polymer-Based High-k Nanocomposites with Suppressed Dielectric Loss and Low Percolation Threshold. *Nanoscale* **2014**, *6*, 14740−14753.
(29) Matyjaszewski, K.; Xia, J. H. Atom Transfer Radical Polymerization. *Chem. Rev.* **2001**, *101*, 2921−2990.
(30) Min, K.; Jakubowski, W.; Matyjaszewski, K. AGET ATRP in the Presence of Air in Miniemulsion and in Bulk. *Macromol. Rapid Commun.* **2006**, *27*, 594−598.
(31) Wang, J. S.; Matyjaszewski, K. Controlled/"Living" Radical Polymerization. Atom Transfer Radical Polymerization in the Presence of Transition-Metal Complexes. *J. Am. Chem. Soc.* **1995**, *117*, 5614−5615.
(32) Anderson, T. R.; Larsen-Olsen, T. T.; Andreasen, B.; Bottiger, A. P. L.; Carle, J. E.; Helgesen, M.; Bundgaard, E.; Norrman, K.; Andreasen, J. W.; Jørgensen, M.; Krebs, F. C. Aqueous Processing of Low-band-gap Polymer Solar Cells Using Roll-to-Roll Methods. *ACS Nano* **2011**, *5*, 4188−4196.
(33) Min, C.; Yu, D.; Cao, J.; Wang, G.; Feng, L. A Graphite Nanoplatelet/Epoxy Composite with High Dielectric Constant and High Thermal Conductivity. *Carbon* **2013**, *55*, 116−125.
(34) Xie, R.; Zhang, D.; Zhang, X. Y.; Zhou, K. C.; Button, T. W. Gelcasting of Alumina Ceramics with Improved Green Strength. *Ceram. Int.* **2012**, *38*, 6923−6926.
(35) Xie, R.; Zhou, K. C.; Gan, X. P.; Zhang, D. Effects of Epoxy Resin on Gelcasting Process and Mechanical Properties of Alumina Ceramics. *J. Am. Ceram. Soc.* **2013**, *96*, 1107−1112.
(36) Yang, Ke.; Huang, X. Y.; Huang, Y. H.; Xie, L. Y.; Jiang, P. K. Fluoro-Polymer@$BaTiO_3$ Hybrid Nanoparticles Prepared via RAFT Polymerization: Toward Ferroelectric Polymer Nanocomposites with High Dielectric Constant and Low Dielectric Loss for Energy Storage Application. *Chem. Mater.* **2013**, *25*, 2327−2338.
(37) Tang, H. X.; Sodano, H. A. Ultra High Energy Density Nanocomposite Capacitors with Fast Discharge Using $Ba_{0.2}Sr_{0.8}TiO_3$ Nanowires. *Nano Lett.* **2013**, *13*, 1373−1379.
(38) Rahimabady, M.; Mirshekarloo, M. S.; Yao, K.; Lu, L. Dielectric behaviors and high energy storage density of nanocomposites with core−shell $BaTiO_3$@TiO_2 in poly(vinylidene fluoride-hexafluoropropylene). *Phys. Chem. Chem. Phys.* **2013**, *15*, 16242−16248.
(39) Ehrhardt, C.; Fettkenhauer, C.; Glenneberg, J.; Munchgesang, W.; Pientschke, C.; Großmann, T.; Zenkner, M.; Wagner, G.; Leipner, H. S.; Buchsteiner, A.; Diestelhorst, M.; Lemm, S.; Beige, H.; Ebbinghaus, S. G. $BaTiO_3$−P(VDF-HFP) nanocomposite dielectrics-Influence of surface modification and dispersion additives. *Mater. Sci. Eng., B* **2013**, *178*, 881−888.
(40) Wu, S.; Li, W. P.; Lin, M. R.; Burlingame, Q.; Chen, Q.; Payzant, A.; Xiao, K.; Zhang, Q. M. Aromatic Polythiourea Dielectrics with Ultrahigh Breakdown Field Strength, Low Dielectric Loss, and High Electric Energy Density. *Adv. Mater.* **2013**, *25*, 1734−1738.
(41) Zhang, Q. M.; Li, H. F.; Poh, M.; Xia, F.; Cheng, Z. Y.; Xu, H. S.; Huang, C. An All-organic Composite Actuator Material with a High Dielectric Constant. *Nature* **2002**, *419*, 284−287.
(42) Li, Y.; Huang, X. Y.; Hu, Z. W.; Jiang, P. K.; Li, S. T.; Tanaka, T. Large Dielectric Constant and High Thermal Conductivity in Poly(vinylidene fluoride)/Barium Titanate/Silicon Carbide Three-Phase Nanocomposites. *ACS Appl. Mater. Interfaces* **2011**, *3*, 4396−4403.
(43) Wang, D.; Zhou, T.; Zha, J. W.; Zhao, J.; Shi, C. Y.; Dang, Z. M. Functionalized Graphene−$BaTiO_3$/Ferroelectric Polymer Nanodielectric Composites with High Permittivity, Low Dielectric Loss, and Low Percolation Threshold. *J. Mater. Chem. A* **2013**, *1*, 6162−6168.
(44) Tang, H. X.; Lin, Y. R.; Sodano, H. A. Enhanced Energy Storage in Nanocomposite Capacitors Through Aligned PZT Nanowires by Uniaxial Strain Assembly. *Adv. Energy Mater.* **2012**, *2*, 469−476.
(45) Mao, X. J.; Shimai, S. Z.; Dong, M. J.; Wang, S. W. Investigation of New Epoxy Resins for the Gel Casting of Cceramics. *J. Am. Ceram. Soc.* **2008**, *91*, 1354−1356.
(46) Zhu, Y.; Xiao, S.; Shi, Y.; Yang, Y.; Hou, Y.; Wu, Y. A Composite Gel Polymer Electrolyte with High Performance Based on Poly (Vinylidene Fluoride) and Polyborate for Lithium Ion Batteries. *Adv. Energy Mater.* **2014**, *4*, 1−9.
(47) Dang, Z. M.; Wang, H. Y.; Zhang, Y. H.; Qi, J. Q. Morphology and Dielectric Property of Homogenous $BaTiO_3$/PVDF Nanocomposites Prepared via the Natural Adsorption Action of Nanosized $BaTiO_3$. *Macromol. Rapid Commun.* **2005**, *26*, 1185−1189.
(48) Hirose, N.; West, A. R. Impedance Spectroscopy of Undoped $BaTiO_3$ Ceramics. *J. Am. Ceram. Soc.* **1996**, *79*, 1633−1641.
(49) McNeal, M. P.; Jang, S. J.; Newnham, R. E. The Effect of Grain and Particle Size on the Microwave Properties of Barium Titanate ($BaTiO_3$). *J. Appl. Phys.* **1998**, *83*, 3288−3297.
(50) Malyshkina, I. A.; Markin, G. V.; Kochervinskii, V. V. Investigation into the Dielectric Relaxation of Vinylidene Fluoride Copolymers with Hexafluoropropylene. *Phys. Solid State* **2006**, *48*, 1197−1199.
(51) Wang, Q.; Zhu, L. Polymer Nanocomposites for Electrical Energy Storage. *Part B: Polym. Phys.* **2011**, *49*, 1421−1429.
(52) Hu, P. H.; Shen, Y.; Guan, Y. H.; Zhang, X. H.; Lin, Y. H.; Zhang, Q. M.; Nan, C. W. Topological-Structure Modulated Polymer Nanocomposites Exhibiting Highly Enhanced Dielectric Strength and Energy Density. *Adv. Funct. Mater.* **2014**, *24*, 3172−3178.
(53) Calame, J. P. Simulation of Polarization, Energy Storage, and Hysteresis in Composite Dielectrics Containing Nonlinear Inclusions. *J. Appl. Phys.* **2011**, *110*, 054107.
(54) Tomer, V.; Manias, E.; Randall, C. A. High Field Properties and Energy Storage in Nanocomposite Dielectrics of Poly (vinylidene fluoride-hexafluoropropylene). *J. Appl. Phys.* **2011**, *110*, 044170.
(55) Roy, M.; Nelson, J. K.; MacCrone, R. K.; Schadler, L. S.; Reed, C. W.; Keefe, R. Polymer Nanocomposite Dielectrics-the Role of the Interface. *Dielectr. Electr. Insul.* **2005**, *12*, 629−643.
(56) Chu, B. J.; Lin, M. R.; Neese, B.; Zhang, Q. M. Interfaces in Poly (vinylidene fluoride) Terpolymer/ZrO_2 Nanocomposites and Their Effect on Dielectric Properties. *J. Appl. Phys.* **2009**, *105*, 014103.
(57) Lewis, T. J. Interfaces: Nanometric Dielectrics. *J. Phys. D: Appl. Phys.* **2005**, *38*, 202.
(58) Xie, Z. K.; Peng, B.; Meng, S. Q.; Zhou, Y. Y.; Yue, Z. X. High-Energy-Storage Density Capacitors of $Bi(Ni_{1/2}Ti_{1/2})O_3$−$PbTiO_3$ Thin Films with Good Temperature Stability. *J. Am. Ceram. Soc.* **2013**, *96*, 2061−2064.
(59) Chu, B. J.; Zhou, X.; Ren, K. L.; Neese, B.; Lin, M. R.; Wang, Q.; Zhang, Q. M. A Dielectric Polymer with High Electric Energy Density and Fast Discharge Speed. *Science* **2006**, *313*, 334−336.
(60) Hao, X. H.; Zhai, J. W.; Yao, X. Improved Energy Storage Performance and Fatigue Endurance of Sr-Doped $PbZrO_3$ Antiferroelectric Thin Films. *J. Am. Ceram. Soc.* **2009**, *92*, 1133−1135.

DOI: 10.1021/acsami.5b00555
ACS Appl. Mater. Interfaces 2015, 7, 8061−8069